Available online at www.sciencedirect.com

SciVerse ScienceDirect

Journal of the European Ceramic Society 32 (2012) 1091–1098

www.elsevier.com/locate/jeurceramsoc

High permeability Ni–Cu–Zn ferrites through additive-free low-temperature sintering of nanocrystalline powders

J. Mürbe, J. Töpfer *

University of Applied Sciences Jena, Dept. SciTec, Carl-Zeiss-Promenade 2, 07745 Jena, Germany

Received 1 September 2011; received in revised form 16 November 2011; accepted 17 November 2011
Available online 15 December 2011

Abstract

Nanocrystalline Ni–Cu–Zn ferrite powders $Ni_{0.20}Cu_{0.20}Zn_{0.62}Fe_{1.98}O_{3.99}$ were prepared by thermal decomposition of an oxalate precursor. The particle size is 6 nm and 350 nm, respectively, for powders obtained through calcinations at 350 °C or 750 °C. The shrinkage behavior significantly changes with particle size; the temperature of maximum shrinkage rate is $T_{MSR} = 700$ °C for particles of 6 nm size and increases to $T_{MSR} = 880$ °C for particles 350 nm in size. Dense samples with a permeability of $\mu = 780$ are obtained by sintering at 900 °C for 2 h. Mixtures of nanocrystalline and sub-micron powders allow tailoring of the shrinkage behavior. A maximum permeability of $\mu = 840$ is obtained after sintering of a 1:1-mixture at 900 °C. This demonstrates the potential of nanocrystalline ferrites for co-firing without additives at 900 °C and integration of ferrite inductors into LTCC modules.

Keywords: Ferrites; Powder-chemical preparation; Sintering; Magnetic properties; Soft magnets

1. Introduction

Ni–Cu–Zn ferrites are used as standard soft magnetic materials for multilayer ferrite inductors (MLFI) because of their low sintering temperature and good performance up to MHz frequencies.[1–3] The temperature for co-firing multilayer inductor components is restricted to 900 °C because silver is used as metallization. Correlations between the composition of Ni–Cu–Zn ferrites and their sintering behavior and magnetic properties have been investigated[4–8] and optimum compositions for low-temperature ceramic co-firing (LTCC) of multilayer inductors can be selected. A typical feature of low-firing ferrite compositions seems to be a small deficiency of iron oxide, i.e. less than 50 mol% Fe_2O_3 is used in the starting mixture of oxides. Such compositions are referred to as sub-stoichiometric here; their composition typically translates into a spinel formula with less than two Fe per formula unit, e.g. $Ni_{0.20}Cu_{0.20}Zn_{0.62}Fe_{1.98}O_{3.99}$, compared to stoichiometric ferrites with 50 mol% Fe_2O_3 and two Fe per formula unit, e.g. $Ni_{0.20}Cu_{0.20}Zn_{0.60}Fe_2O_4$. It was shown that Fe-deficient sub-stoichiometric compositions exhibit enhanced densification.[9] Additionally, sintering additives are being used in order to enhance shrinkage and densification at 900 °C. Bismuth oxide has frequently been suggested as sintering aid for Ni–Cu–Zn ferrites.[10–12] The addition of <1 wt% of Bi_2O_3 has been shown to be effective for preparing ferrites with a permeability as large as $\mu = 900$.[13,14]

Another approach to obtain dense samples with optimized microstructures after firing at 900 °C is the use of sinter-active ferrite powders prepared by alternative synthesis routes. The precipitation of mixed oxalates and their subsequent thermal decomposition into ferrites is a classic alternative synthesis procedure of nanocrystalline ferrite particles.[15] The oxalate route was already used to synthesize various nanocrystalline ferrite powders, e.g. magnetite,[16] Mn–Zn ferrites,[17,18] and Ni–Cu–Zn ferrites.[19]

In this contribution, we report on a systematic investigation of the synthesis and morphology of nanocrystalline Ni–Cu–Zn ferrite particles via the oxalate precursor route. We have studied the shrinkage, sintering behavior and microstructure formation upon firing at 900 °C. The permeability of the sintered samples was investigated as function of the powder particle

* Corresponding author. Tel.: +49 3641 205479; fax: +49 3641 205451.
E-mail address: joerg.toepfer@fh-jena.de (J. Töpfer).

0955-2219/$ – see front matter © 2011 Elsevier Ltd. All rights reserved.
doi:10.1016/j.jeurceramsoc.2011.11.021

size, and compared to that of ferrites made from standard submicron powders. The effect of dwell time during sintering at 900 °C on grain size and permeability is studied. Moreover, the potential of powder mixtures of nanocrystalline and submicron powders is evaluated. This method was already reported by Su et al. using nanocrystalline Ni–Cu–Zn ferrite synthesized via a sol–gel route.[20] However, no detailed information on individual powder particle sizes was reported. Moreover, the powder mixture was wet-milled until the average particle size was below 1 μm using stainless steel balls. The wear from the grinding media used in Ref. 20 is very likely to have increased the iron content upon milling and modified the ferrite composition and, hence, sintering behavior and permeability. It is demonstrated here, that the addition of nanocrystalline to sub-micron standard ferrite powders can be understood as application of an "internal" sintering aid. This is an approach to develop "external" (e.g. Bi_2O_3) additive-free Ni–Cu–Zn ferrites for integrated multilayer inductors. It has been shown, that the addition of Bi_2O_3 sintering aid to ferrites might have dramatic effects on the microstructure formation and hence permeability of Ni–Cu–Zn ferrite multilayer structures integrated into LTCC modules.[21]

2. Experimental

Ferrite powders of composition $(NiO)_{0.20}(CuO)_{0.20}(ZnO)_{0.62}(Fe_2O_3)_{0.99}$, i.e. $Ni_{0.20}Cu_{0.20}Zn_{0.62}Fe_{1.98}O_{3.99}$, were prepared by the oxalate precursor route. Fe-powder was dissolved in acetic acid under Ar-atmosphere to avoid the formation of Fe^{3+}, a procedure already proposed by Wickham.[15] Ni-, Cu-, and Zn-acetate-hydrates were dissolved in water and this mixed metal solution was added to the Fe-(II)-acetate solution. This mixed-cation solution is added to an oxalic acid solution in an argon atmosphere and a mixed-metal oxalate precipitate is formed. Co-precipitation and ageing for 2 h was performed at room temperature and at 70 °C. The oxalate powder is dried by removing the liquid in a rotary evaporator at 60 °C. The thermal decomposition of the mixed-metal oxalate was performed between 350 and 750 °C in Pt-containers without lids (powders referred to as oxalate350, . . ., 750).

A standard ferrite powder was prepared by the mixed-oxide route (powder oxide750). α-Fe_2O_3 (TKS Germany, HP grade) with a specific surface $S = 4.3\ m^2/g$; NiO (Inco, Black Nickel Oxide, Grade F) with $S = 70\ m^2/g$; CuO p. A. (Merck, Germany) with $S = 4.6\ m^2/g$ and ZnO (Harzsiegel Heubach, Germany, standard grade) with $S = 4.5\ m^2/g$ were used as starting materials. The oxides were wet mixed for 12 h in a polyethylene container. After drying the powder was calcined at 750 °C for 2 h and subsequently milled in a planetary ball mill using zirconia grinding media. Powder mixtures of nanocrystalline (oxalate350) and sub-micron (oxide750) powders were homogenized in a rotating PE container using water and zirconia grinding media (1 mm diameter) for 24 h. The ferrite powders were compacted using polyvinyl-alcohol as binder to give pellets for sintering studies or toroids for permeability measurements. The sintering was performed at 900 °C in air with a heating rate of 2 K/min up to 450 °C and 10 K/min to 900 °C and dwell times at 900 °C of 2, 4, or 12 h, respectively.

The phase formation of the materials was evaluated by XRD (Siemens D5000). The particle size of the powders was measured in an aqueous suspension using a laser diffraction system (Malvern Mastersizer 2000). The specific surface S of the powders was determined by nitrogen adsorption (BET, Nova 2000, Quantachrome Instruments, Boynton Beach, USA); a mean particle size (assuming spherical particles) was estimated using the relation $d_{BET} = 6/\rho \cdot S$ with the density ρ. The crystallite size was estimated from XRD line broadening using the Scherrer equation, $d_{xrd} = K\lambda/[(B - b)\cos\theta]$, with the wave length λ, the peak width B, the instrumental broadening b ($b = 0.08°$ for standard LaB_6), the Bragg angle θ and the shape factor $K \approx 0.89$. Thermal analysis (TG, DTA) was carried out with a SETARAM TGA92 system, the samples were heated in open Pt containers (TG + DTA sample holder: diameter 3 mm, height 6 mm) in air with a rate of 2 K/min (sample mass about 20 mg). Shrinkage measurements were made with a Netzsch DIL402 dilatometer on cylindrical compacts during heating to 1000–1200 °C with 4 K/min heating rate. The bulk density of sintered samples was determined from the dimensions and weight. The powder morphology and the microstructure of the sintered samples were studied with a scanning electron microscope (SEM, Zeiss DSM940A). The permeability of the sintered toroids was measured using an impedance analyzer in the frequency range 1–1000 kHz. For frequencies up to 2 GHz permeability measurements were performed using an Agilent E4991A impedance/materials analyzer.

3. Results and discussion

3.1. Synthesis of nanocrystalline Ni–Cu–Zn ferrite powders

The co-precipitated Ni–Cu–Zn-Fe oxalate hydrates are yellowish powders with an orthorhombic β-oxalate structure as shown by X-ray diffraction (not shown here). Thermal decomposition of the mixed oxalate hydrate in air is almost complete at 300 °C (Fig. 1). The DTA curve exhibits an endothermic peak at 150 °C as signature of the dehydration step and an exothermic peak at 270 °C corresponding to the oxalate decomposition reaction. The temperature of Ni–Cu–Zn–Fe oxalate precipitation has a dramatic influence on the particle morphology. Whereas mixed oxalates precipitated at room temperature exhibit a homogeneous particle size of about 0.5 μm with little formation of hard aggregates (Fig. 2a), the mixed-metal oxalates precipitated and aged at 70 °C form 2 μm large star-like aggregates (Fig. 2b). The oxalate aggregate morphology is kept during the thermal decomposition process. The morphology of the decomposition products is similar to those of the oxalates (Fig. 2c and d). This topotactic transformation behavior is typical of precursor decompositions and was already reported for other oxalate to ferrite transformations.[16,18] Since a fine-grained oxide powder is obtained only through thermal decomposition of oxalate particles precipitated at room temperature, the following studies were performed with these mixed-metal oxalates.

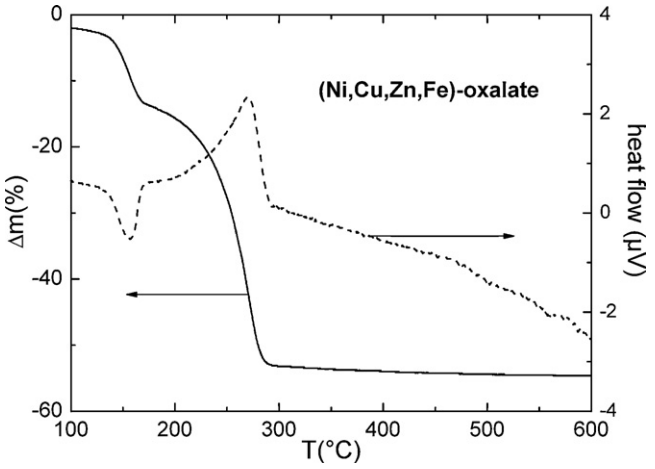

Fig. 1. TG and DTA curves of Ni–Cu–Zn-Fe oxalate (prepared by coprecipitation at 25 °C) annealed in air with 10 K/min.

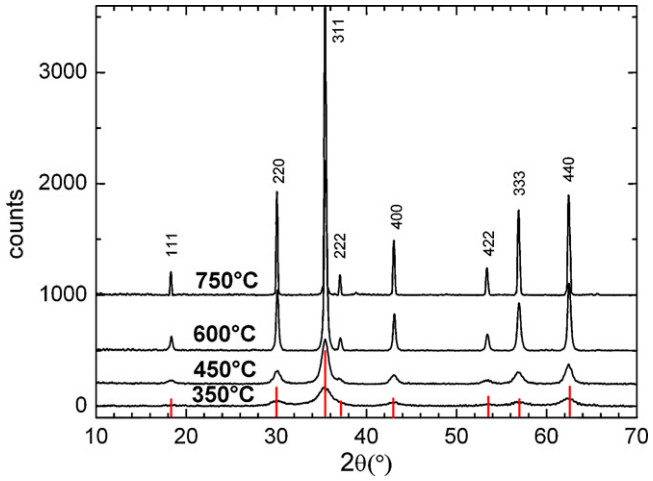

Fig. 3. XRD patterns of Ni–Cu–Zn ferrites prepared through thermal decomposition of mixed-metal oxalate at 350, 450, 600, and 750 °C.

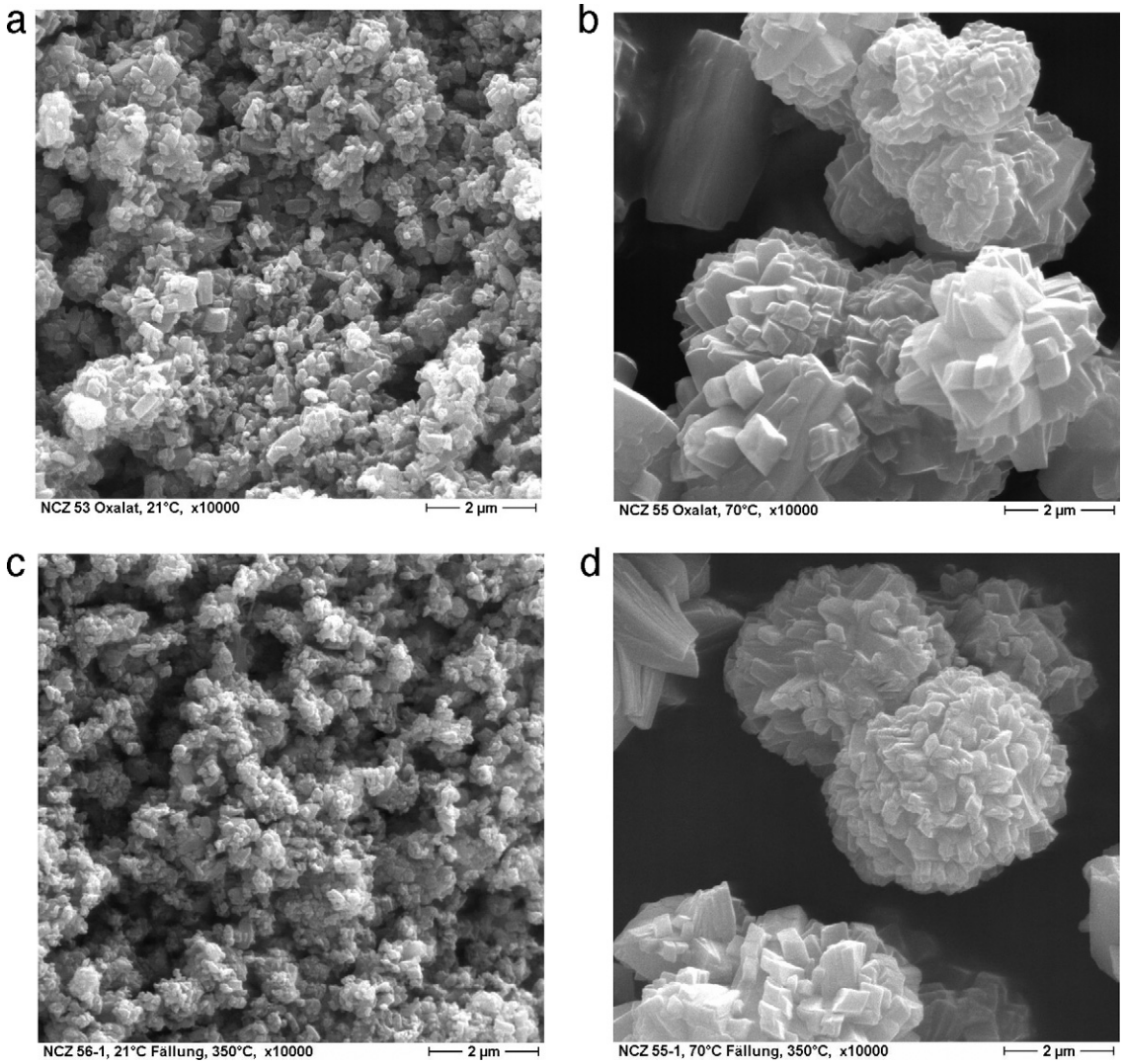

Fig. 2. SEM micrographs of mixed-metal oxalates coprecipitated at 25 °C (a) or 70 °C (b), and ferrite powders prepared by thermal decomposition at 350 °C of mixed-metal oxalates coprecipitated at 25 °C (c) or 70 °C (d).

Table 1
Morphological properties of ferrite powders synthesized by thermal decomposition of Ni–Cu–Zn–Fe oxalates at 350–750 °C in air (specific surface area S, particle diameter from specific surface d_{BET}; crystallite size d_{xrd}).

T (°C)	S (m^2/g)	d_{BET} (nm)	d_{XRD} (nm)
350 °C/2 h	193	6	7(2)
450 °C/2 h	70.9	16	11(2)
600 °C/2 h	18.3	60	41(10)
750 °C/2 h	3.2	350	250

Samples of the Ni–Cu–Zn–Fe oxalate were calcined at 350, 450, 600, and 750 °C for 2 h in air, respectively. XRD analysis of the decomposition products (Fig. 3) reveals the formation of a single-phase spinel-type ferrite at all temperatures. The powder formed at 350 °C exhibits broad diffraction peaks indicating a nanocrystalline ferrite particle size. With increasing temperature of oxalate decomposition the peak widths become smaller. The crystallite size d_{XRD} of the ferrites calculated using the Scherrer equation is documented in Table 1. Calcinations of the mixed oxalate at 350 °C indeed results in the formation of a nanocrystalline ferrite powder with a crystallite size of $d_{XRD} = 7$ nm and a mean primary particle size of $d_{BET} = 6$ nm. Calcination of the mixed oxalate at higher temperature leads to growth of the ferrite particles; e.g. calcinations at 600 °C gives particles with $d_{XRD} = 41$ nm and $d_{BET} = 60$ nm (Table 1). SEM micrographs (Fig. 2c) illustrate that the ferrite powder, topotactically formed through oxalate decomposition, consists of porous aggregates of nanocrystalline ferrite particles. However, the aggregates are hardly agglomerated.

For comparison, a Ni–Cu–Zn ferrite powder of identical composition $Ni_{0.20}Cu_{0.20}Zn_{0.62}Fe_{1.98}O_{3.99}$ was prepared through the mixed-oxide route (powder oxide750). An aggregate size of $d_{50} = 0.6$ μm was measured by laser diffraction after calcinations at 750 °C and fine-milling. The specific surface of that powder is $S = 14$ m^2/g corresponding to a mean particle diameter of $d_{BET} = 80$ nm. On the other hand, fine milling of the calcined powder has led to hard aggregates (as measured by laser diffraction to $d_{50} = 0.6$ μm and clearly visible in SEM micrographs), hence the powder oxide750 is rather considered as a typical sub-micron powder.

3.2. Sintering behavior of nanocrystalline Ni–Cu–Zn ferrite powders

Dilatometric shrinkage measurements performed on pellets made of nanocrystalline powders (Fig. 4a and b) demonstrate that the shrinkage behavior is quite different for ferrite powders synthesized through oxalate decomposition at different temperatures: (i) the onset of shrinkage is at $T < 400$ °C for ferrite powders with $d_{BET} = 6$ nm (oxalate350) and increases to about 700 °C for powders with $d_{BET} = 350$ nm (oxalate750); (ii) the absolute shrinkage decreases from 30% for the nanocrystalline powder oxalate350 with $d_{BET} = 6$ nm to about 18% for the sub-micron powder oxalate750 with $d_{BET} = 350$ nm; and (iii) the temperature of the maximum shrinkage rate is shifted from $T_{MSR} = 880$ °C for sub-micron powders with $d_{BET} = 350$ nm

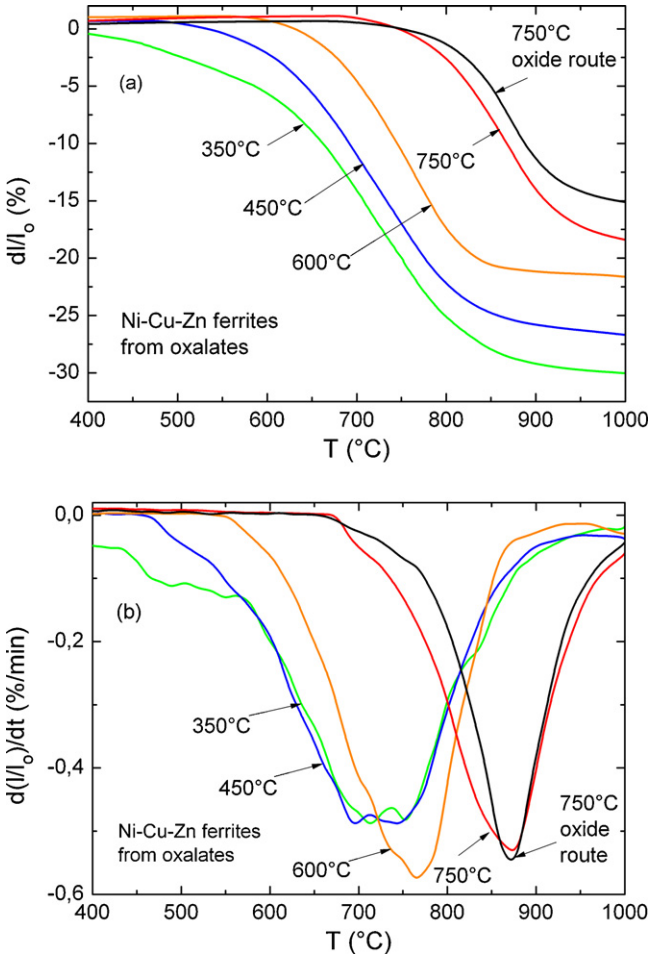

Fig. 4. Shrinkage (a) and shrinkage rate (b) of Ni–Cu–Zn ferrite powders prepared by thermal decomposition of mixed-metal oxalates at 350, 450, 600, and 750 °C compared to a submicron-sized ferrite powder prepared via the mixed-oxide route and fine milling (oxide750).

(oxalate750) down to about $T_{MSR} = 700$ °C for nanocrystalline powders with $d_{BET} = 6$ nm (oxalate350) (Fig. 4b). The shrinkage curves of the ferrite powders obtained through the oxalate route are compared to that of a ferrite obtained through the mixed-oxide route. Powder oxide750 exhibits a shrinkage behavior similar to that of powder oxalate750 obtained through oxalate decomposition at 750 °C. This is somewhat surprising since the mean primary particle size of the powder oxide750 ($d_{BET} = 80$ nm) is smaller compared to that of oxalate750 ($d_{BET} = 350$ nm), but the aggregation behavior of the former results in quite a large number of hard aggregates which dominate the morphology of this sub-micron powder.

Sintering experiments at 900 °C were performed using nanocrystalline Ni–Cu–Zn ferrite powders prepared via thermal decomposition of mixed-metal oxalates at 350 °C (powder oxalate350). For comparison samples of the submicron powder prepared via the mixed-oxide route (oxide750) were studied. Samples of the nanocrystalline powder (oxalate350) sintered at 900 °C exhibit a high density (>98%) which does not change with dwell time (Fig. 5). Samples of the sub-micron powder oxide750 also sinter to high density, however, their densities are somewhat lower compared to those of samples from powder

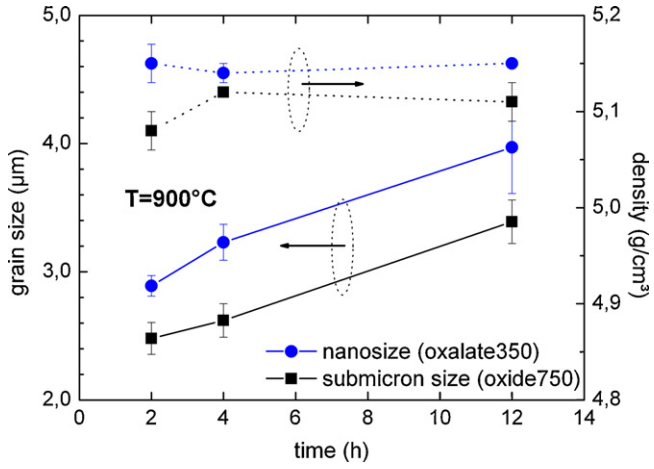

Fig. 5. Grain size and density after sintering at 900 °C as function of dwell time for Ni–Cu–Zn ferrites prepared from nanocrystalline (oxalate350) and submicron-size ferrite powders (oxide750).

oxalate350. This demonstrates the excellent sinter-activity of the nanocrystalline ferrite powder. The grain size of the samples sintered at 900 °C is also shown in Fig. 5 as function of dwell time. As expected, the grain size of both sample series increases with dwell time, but the grain sizes of the sintered samples made of nanocrystalline powder (oxalate350) are larger. Grain growth seems to proceed faster due to the high density of the samples and lower resistance to grain boundary motion. The larger grain size of ceramics made from nanocrystalline ferrite powders is demonstrated in SEM micrographs of samples sintered at 900 °C for 4 h (Fig. 6).

3.3. Magnetic properties

The larger grain size of samples made from nanocrystalline powder (oxalate350) is reflected in a larger permeability (Fig. 7a). Samples from nanocrystalline Ni–Cu–Zn ferrite powders exhibit permeabilities of $\mu = 780$ and 980 after sintering at 900 °C for 2 and 12 h, respectively (Fig. 7a). Although the two sample sets (oxalate350 and oxide750) display different grain sizes, an almost linear correlation between permeability and grain size is observed. This indicates that the permeability is dominated by domain wall motion. It has been demonstrated that for this magnetization mechanism μ is a linear function of grain size (Globus model).[22,23] The fact that the permeability of samples with grain size of 2–3 μm linearly increases with grain size signals that the grains contain domain walls and are of multi-domain type. The analysis of permeability spectra of Ni–Cu–Zn ferrites has shown that up to 10 MHz domain wall motion as well as spin rotation contribute to the magnetization process; at higher frequency spin rotation becomes dominating.[24] A similar linear relationship between permeability and grain size was already observed for Ni–Cu–Zn ferrites with and without Bi_2O_3 additive.[25] In the former case, due to inhomogeneous grain growth, the grain size is between 10 and 50 μm and hence the permeability is larger.

The permeability as function of frequency of Ni–Cu–Zn ferrite sintered at 900 °C for 2 h from nanocrystalline powder

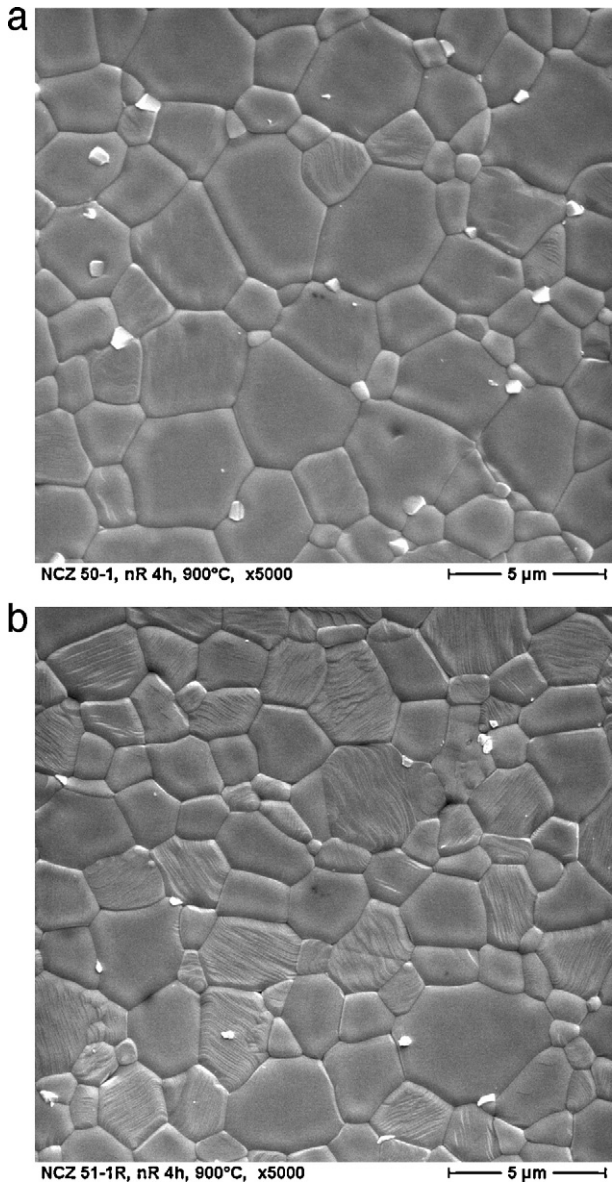

Fig. 6. SEM micrographs of Ni–Cu–Zn ferrites sintered for 4 h at 900 °C made from a nanocrystalline (oxalate350) and a submicron-size ferrite powder (oxide750).

(oxalate350) is shown in Fig. 7b. A permeability of $\mu = 780$ is observed independent of frequency up to 1 MHz. At higher frequency the permeability declines and a resonance frequency f_R (maximum of imaginary part of permeability, μ''_{max}) appears at 3 MHz. The ferrite made from submicron powder oxide750 has a lower permeability of $\mu = 670$ with a somewhat higher $f_R = 4$ MHz. Both samples display a product of $\mu \cdot f_R$ of around 3 GHz which is in fair agreement with values reported for conventionally sintered Ni–Zn ferrites with similar grain size.[23] The permeability spectra $\mu''(f)$ are unsymmetrical in shape; moreover the maximum value of μ'' does not cross the $\mu'(f)$ curve. This might be interpreted as being due to a rather broad distribution of different grain sizes[26] which indeed is confirmed by the SEM micrographs (Fig. 6). However, these results demonstrate

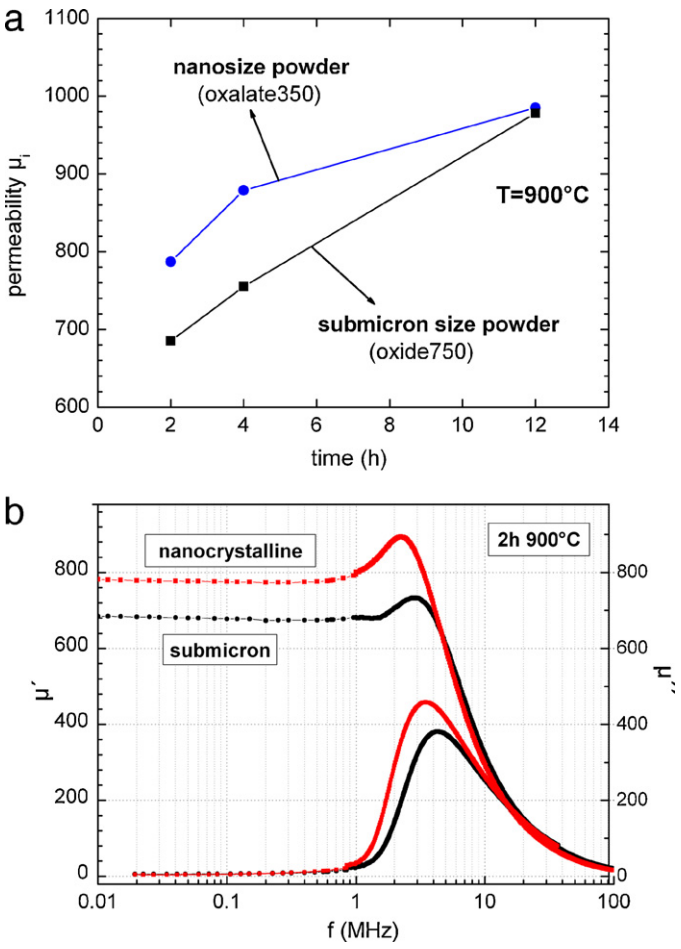

Fig. 7. Permeability μ_i (μ at 1 MHz) after sintering at 900 °C as function of dwell time (a) and permeability vs. frequency (b) for Ni–Cu–Zn ferrites prepared from nanocrystalline (oxalate350) and submicron-size powders (oxide750).

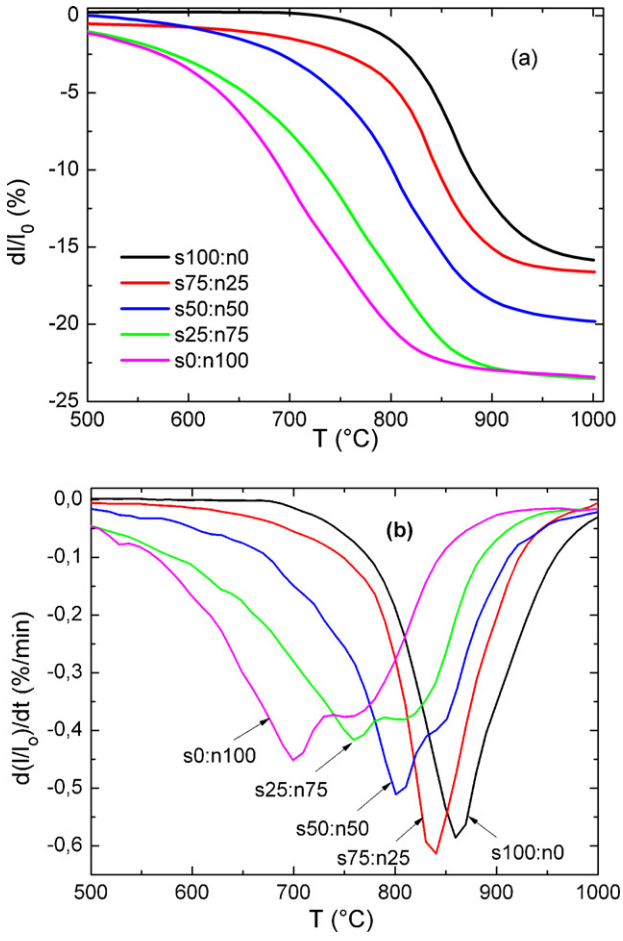

Fig. 8. Shrinkage (a) and shrinkage rate (b) vs. temperature of compacts of Ni–Cu–Zn ferrite powder mixtures prepared from nanocrystalline (oxalate350) and submicron-size (oxide750) powders; mixing ratio of submicron:nanocrystalline powders (s:n) in wt%.

that ferrites made from nanocrystalline powders exhibit excellent densification and grain growth characteristics after firing for 2 h at 900 °C. This is a typical sintering profile for multilayer inductors. Usually, submicron ferrite powders are used in combination with sintering additives in order to achieve complete densification after sintering at 900 °C. Bi_2O_3, for example, is a popular additive for multilayer ferrites and a permeability of $\mu = 900$ was reported for additive concentrations as low as 1 wt%.[13,14] The results presented in this study demonstrate that additive-free Ni–Cu–Zn ferrites can be sintered to high density and permeability. This might be advantageous, since additives at certain critical concentrations usually trigger exaggerated grain growth. This turns the co-firing of MLFIs into a process step which is difficult to control. Moreover, it was shown that Bi_2O_3 additives might pose problems during the integration of ferrite layers into LTCC modules because of the mobility and volatility of Bi.[21] Grain growth significantly depends on the Bi-concentration[13] and different Bi-concentrations in the interior and boundary regions of ferrite layers embedded in standard LTCC tapes were observed.[21] These difficulties might be circumvented by the use of additive free ferrite systems.

3.4. Nanocrystalline/submicron ferrite powder mixtures

Finally, the potential of mixtures of nanocrystalline and sub-micron powders is evaluated. The shrinkage and shrinkage rate of mixtures of different concentrations of oxalate350 and oxide750 powders are shown in Fig. 8. With increasing amount of nanocrystalline powder the onset of shrinkage is shifted towards lower temperatures, the absolute shrinkage is increased, and the temperature of maximum shrinkage rate is decreased. The densities of powder mixtures before and after sintering are summarized in Table 2. The green density of

Table 2
Green density, sintered density after firing 2 h at 900 °C, and permeability μ_i (μ at 1 MHz) for Ni–Cu–Zn ferrites made from mixtures of nanocrystalline (oxalate350) and submicron-size (oxide750) powders.

Sub:nano (wt%)	ρ_{green} (g/cm^3)	$\rho_{sintered}$ (g/cm^3)	μ_i
100:0	3.22(1)	5.10(1)	670
75:25	3.10(1)	5.28(2)	690
50:50	2.85(1)	5.22(2)	840
25:75	2.64(3)	5.19(2)	795
0:100	2.44(1)	5.12(3)	780

uniaxially pressed compacts decreases with increasing concentration of nanoparticles. This poor densification of nanopowders during consolidation is reflected in the large shrinkage of these compositions (Fig. 8). After sintering at 900 °C all samples exhibit high densities, however, maximum densities are observed for mixtures with 25 or 50 wt% nanocrystalline powder (oxalate350). The permeability of the sintered samples has a maximum value of $\mu = 840$ for the 1:1 mixture of nanocrystalline and submicron powders. This is caused by the maximum density of that particular mixing ratio as well as the fact that this composition shows a quite homogeneous microstructure with grains of size of 2–3 μm. The application of nanocrystalline ferrite powders as additives to regular ferrite powders was already reported by Su et al.[20] using nanocrystalline Ni–Cu–Zn ferrite synthesized via a sol–gel route. However, no detailed information on individual powder particle sizes was given, and the powder mixture was wet-milled until the average particle size was below 1 μm using stainless steel balls which might induce problems due to wear of the grinding media and modifications in ferrite composition and, consequently, the sintering behavior and permeability too. It is demonstrated here, that the addition of nanocrystalline to sub-micron standard ferrite powders can be understood as application of an "internal" sintering aid. This approach can be further optimized to develop "external" additive-free Ni–Cu–Zn ferrites for integrated multilayer inductors. This will prove advantageous for the co-firability, microstructure formation and hence permeability of Ni–Cu–Zn ferrite multilayer structures integrated in LTCC modules. The possibility of tailoring of the ferrite shrinkage curve by addition of nanocrystalline powder is an interesting option to reduce the shrinkage mismatch between ferrite and dielectric tapes and to enable successful co-firing of both materials for integrated inductive components in LTCC modules.

4. Conclusions

Nanocrystalline Ni–Cu–Zn ferrite powders were synthesized through an oxalate-based precursor process. The ferrite particle size is tailored by calcinations of the oxalate precursor at temperatures between 350 and 750 °C. The obtained ferrite particles exhibit interesting properties which can be used to obtain optimized multilayer inductors:

1) With increasing particle size the temperature of the maximum shrinkage rate is shifted from $T_{MSR} = 700$ °C for $d = 6$ nm towards $T_{MSR} = 880$ °C for a powder with $d = 350$ nm. A similar effect is observed for mixtures between nanocrystalline and standard sub-micron ferrite powders; the maximum shrinkage rate is shifted towards lower temperatures upon addition of nanocrystalline particles. This effect can be used to tailor the shrinkage behavior of ferrite tapes and to reduce the shrinkage mismatch during co-firing with LTCC tapes.
2) Sintering of nanocrystalline ferrite powders at 900 °C leads to almost complete densification. Compared to standard sub-micron powders, enhanced grain growth gives rise to increased permeability. A large permeability of $\mu = 780$ was found for a sample made from nanocrystalline ferrite powder synthesized by oxalate decomposition at 350 °C. An even larger permeability of $\mu = 840$ was observed using a mixture of nanocrystalline and submicron powders.
3) Nanocrystalline ferrite powders might be used as "internal" sintering additives for sub-micron Ni–Cu–Zn ferrites for optimized shrinkage behavior and microstructure formation.

Acknowledgement

This work was supported by the Bundesministerium für Bildung und Forschung (Germany) through the grant NIKOL (03X45003F).

References

1. Nomura T, Nakano A. New evolution of ferrites for multilayer chip components. In: *Proc. of the sixth international conference on ferrites*. 1992. p. 1198–201.
2. Nakamura T, Okano Y. Low temperature sintered Ni–Zn–Cu ferrite. *J Phys IV France* 1997;**7**(C1):91–2.
3. Yasuda K, Mochizuki Y, Takaya M. Multilayer ferrite chip component for growth of microelectronics. In: *Proc. of the eight international conference of ferrites*. 2000. p. 1162–4.
4. Byeon SC, Je HJ, Hong KS. Microstructural optimization of low-temperature fired Ni–Zn–Cu ferrites using calcinations. *Jpn J Appl Phys* 1997;**36**:5103–8.
5. Nakano A, Nomura T. Multilayer chip inductors. *Ceram Transact* 1999;**97**:285–304.
6. Low KO, Sale FR. The development and analysis of property-composition diagrams on sol–gel derived stoichiometric NiCuZn ferrite. *J Magn Magn Mater* 2003;**256**:221–6.
7. Murthy S. Low temperature sintering of NiCuZn ferrite and its electrical, magnetic and elastic properties. *J Mater Sci Lett* 2002;**21**:657–60.
8. Mürbe J, Töpfer J. Ni–Cu–Zn ferrites for low temperature firing: I. Ferrite composition and its effect on sintering behavior and permeability. *J Electroceramics* 2005;**15**:215–21.
9. Mürbe J, Töpfer J. Low temperature sintering of sub-stoichiometric Ni–Cu–Zn ferrites: shrinkage, microstructure and permeability. *J Magn Magn Mater* 2012;**324**:578–83.
10. Hsu JY, Ko WS, Shen HD, Chen YJ. Low temperature fired NiCuZn ferrite. *IEEE Trans Magn* 1994;**30**:4875–7.
11. Jean JH, Lee CH. Low-fire NiO–CuO–ZnO Ferrite with Bi_2O_3. *Jpn J Appl Phys* 1999;**38**:3508–12.
12. Wang SF, Wang YR, Yang T, Chen CF, Lu CA, Huang CY. Densification and magnetic properties of low-fire NiCuZn ferrites. *J Magn Magn Mater* 2000;**220**:129–38.
13. Mürbe J, Töpfer J. Ni–Cu–Zn Ferrites for low temperature firing: II. Effects of powder morphology and Bi_2O_3 addition on microstructure and permeability. *J Electroceramics* 2006;**16**:199–205.
14. Jeong J, Han YH, Moon B. Effects of Bi_2O_3 addition on the microstructure and electromagnetic properties of NiCuZn ferrites. *J Mater Sci: Mater Electronics* 2004;**15**:303–6.
15. Wickham DG. Metal-iron-(III)-oxides. *Inorg Synth* 1967;**9**:152–6.
16. Angermann A, Töpfer J. Synthesis of magnetite nanoparticles by thermal decomposition of ferrous oxalate dihydrate. *J Mater Sci* 2008;**43**: 5123–30.
17. Bremer M, Fischer S, Langbein H, Töpelmann W, Scheler H. Investigation on the formation of manganese zinc ferrites by thermal decomposition of solid solution oxalates. *Thermochim Acta* 1992;**209**: 323–30.
18. Angermann A, Töpfer J. Synthesis of nanocrystalline Mn–Zn ferrite powders through thermolysis of mixed oxalates. *Ceram Intl* 2011;**37**: 995–1002.

19. Ghodake SA, Ghodake UR, Sawant SR, Suryavanshi SS, Bakare PP. Magnetic properties of NiCuZn ferrites synthesized by oxalate precursor method. *J Magn Magn Mater* 2006;**305**:110–9.
20. Su H, Zhang H, Tang X, Liu Y. Effects of nanocrystalline ferrite partuicles on densification and magnetic properties of NiCuZn ferrites. *J Mater Sci* 2007;**42**:2849–53.
21. Rabe T, Naghib-zadeh H, Glitzky C, Töpfer J. Integration of Ni–Cu–Zn ferrite in LTCC modules. In: *Proc. 7th international conference on ceramic interconnect and ceramic microsystems technologies*. 2011.
22. Globus A, Duplex P. Separation of susceptibility mechanisms for ferrites of low anisotropy. *IEEE Trans Magn* 1966;**2**:441–5.
23. Lebourgeois R, Le Fur C, Labeyrie M, Pate M, Ganne JP. Permeability mechanisms in high-frequency polycrystalline ferrites. *J Magn Magn Mater* 1996;**160**:329–32.
24. Nakamura T. Low temperature sintering of Ni–Cu–Zn ferrite and its permeability spectra. *J Magn Magn Mater* 1997;**168**:285–91.
25. Töpfer J, Mürbe J, Müller E, Bechtold F. Sintering behavior of Ni–Cu–Zn Ferrites for multilayer inductors. *Ceram Transact* 2006;**174**:225–35.
26. Jankovskis J. Presentation of complex permeability spectra of polycrystalline ferrites based on grain size distribution. *J Magn Magn Mater* 2004;**272–276**:e1847–9.